Research in Astronomy and Astrophysics, 22:085021 (9pp), 2022 August https://doi.org/10.1088/1674-4527/ac7a98

On the Jet Structures of GRB 050820A and GRB 070125

Xin-Yu Li[1,2], Hao-Ning He[1,2], and Da-Ming Wei[1,2]
[1] Key Laboratory of Dark Matter and Space Astronomy, Purple Mountain Observatory, Chinese Academy of Sciences, Nanjing 210033, China; dmwei@pmo.ac.cn, hnhe@pmo.ac.cn
[2] School of Astronomy and Space Science, University of Science and Technology of China, Hefei 230026, China
Received 2022 April 6; revised 2022 June 7; accepted 2022 June 14; published 2022 July 22

Abstract

We present the broadband numerical modeling of afterglows for two remarkably bright long gamma-ray bursts (GRBs), GRB 050820A and GRB 070125, with a wide range of observations from the radio band to the X-ray band. In our work, we fit light curves and constrain physical parameters using a standard forward shock model from the `afterglowpy` `Python` package, considering different jet structures and the jet lateral expansion. For GRB 050820A, the constrained jet is close to a top-hat jet with an extremely small half opening angle of about 0.015 rad, and the circumburst matter density is as small as 10^{-7} cm^{-3}, which suggests that this peculiar long GRB might originate from metal-poor stars with low mass-loss rates. To explain the late time optical light curves of GRB 070125, the effects of the lateral expansion and the participation factor of electrons that are accelerated by the shock have to be taken into account. The constrained results for GRB 070125 show that the jet is also close to a top-hat jet with a half opening angle of about 0.1 rad, the viewing angle is about 0.05 rad, the circumburst density is about 10 cm^{-3}, and the participation factor is about 0.1. The jet energy of the two bursts is required to be $\sim 10^{51}$–10^{52} erg, which can be produced by a millisecond magnetar or a hyper-accreting black hole.

Key words: methods: numerical – ISM: jets and outflows – gamma-rays: ISM – gamma-rays: general

1. Introduction

Gamma-ray bursts (GRBs) originate from the collapse of massive stars or the merger of compact stars, which are the brightest explosive events in the universe. After collapsing or merging, collimated ultra-relativistic jets emerge from the central engine, which might be powered by the rotation energy of a central magnetar (Uso 1992) or the accretion of star material onto a central black hole (Woosley 1993). As the jet propagates through the external medium, its interaction with the medium will produce multi-wavelength afterglow emission. The highly collimated jets can explain the extremely high isotropic energy of GRBs and the jet break phenomenon of the afterglow emission (Sari et al. 1999; Rhoads 1999). In nature, most GRB jets might be structured jets. Besides the top-hat jet model, there are also more complex jet models such as the Gaussian model and the power-law model that are widely discussed. If jets are viewed on-axis, the light curves of structured jets are similar to those of top-hat jets. If viewed off-axis, light curves of structured jets display more complex behavior than top-hat jets (Kumar & Granot 2003; Wei & Jin 2003).

In 2017, the binary neutron-star merger event GW170817 was observed followed by a GRB, GRB 170817A (Abbott et al. 2017a, 2017b). The afterglow of GRB 170817A demonstrates quite a few characteristics different from typical afterglows, such as the lack of early emission, a slow rising light curve, apparent motion of the radio centroid and post-break sharp decline, which are consistent with a structured jet viewed off-axis (Lamb & Kobayashi 2017; Alexander et al. 2018; Hotokezaka et al. 2018; Wu & MacFadyen 2018; Ghirlanda et al. 2019; Fong et al. 2019; Lamb et al. 2019; Troja et al. 2019; Mooley et al. 2018; He et al. 2018). Ryan et al. (2020) developed an open source `Python` package `afterglowpy` to compute the afterglow emission from structured jets from different viewing angles to explain characteristics of light curves for GRB 170817A.

Cunningham et al. (2020) used the `afterglowpy` software package to analyze the afterglow for GRB 160625B, a long GRB with a high isotropic energy $E_{\gamma,\rm iso} \sim 10^{54}$ erg (Burns 2016) and redshift $z = 1.406$ (Xu et al. 2016), and concluded that a Gaussian-shaped jet is favored over a top-hat jet (Cunningham et al. 2020).

To find more evidence of structured jets, we pick two bursts, GRB 050820A at $z = 2.615$ (Prochaska et al. 2005; Ledoux et al. 2005) and GRB 070125 at $z = 1.547$ (Cenko et al. 2008), to analyze their afterglow behavior. These two bursts are analogous to GRB 160625B for their very high isotropic energy, high redshift and abundant multi-wavelength afterglow observations.

Previous works analyzed the multi-wavelength afterglow observations of GRB 050820A (Cenko et al. 2006) and GRB 070125 (Updike et al. 2008; Chandra et al. 2008), using uniform jet models. Cenko et al. (2006) simply adopted a power-law relation $F_\nu \propto t^{-\alpha}\nu^{-\beta}$ to fit the light curve and

spectra for the afterglow of GRB 050820A. Chandra et al. (2008) performed an afterglow analysis on GRB 070125, but reported some parameters with unreasonable values.

In this work, we make use of the `afterglowpy` package for multi-wavelength afterglow modeling of GRB 050820A and GRB 070125, to study jet structures such as the top-hat, Gaussian and power-law jet models, the fraction of electrons that are accelerated by the shock, i.e., the participation fraction ξ_N (in most previous studies, it was often assumed that all electrons have been accelerated to high energy, however in reality it is possible that only a fraction of electrons could be accelerated to high energy by the shock) and the lateral expansion (LE) of jets. In our work, we leave the viewing angle θ_v as a free parameter, while $\theta_v = 0$ is fixed in previous works. Posterior distributions of physical parameters are generated by adopting a Markov Chain Monte Carlo (MCMC) ensemble sampler `emcee` `Python` package (Foreman-Mackey et al. 2013). In the end, we evaluate jet structures and central engines of the two GRBs.

In Section 2, we introduce the `afterglowpy` model and mathematical definitions of jet models. We present the detailed analyses of GRB 050820A and GRB 070125 in Section 3 and Section 4, respectively. Discussions and conclusions are presented in Section 5. Cosmological parameters are adopted as $H_0 = 67.4 \pm 0.5\,\mathrm{km\,s^{-1}\,Mpc^{-1}}$ and $\Omega_m = 0.315 \pm 0.007$ (Aghanim et al. 2020) throughout the paper.

2. `Afterglowpy`

`Afterglowpy` is a public `Python` package, which implements the single-shell approximation to model a blast wave propagating through a uniform circumburst medium, to calculate the afterglow emission from the forward shock for different viewing angles and jet structures. Different variations of jet structures, such as the top-hat, Gaussian and power-law jet models, are included.

To the present time, the top-hat jet, i.e., a uniform jet, is most frequently used in GRB problems. The following function describes the energy distribution as a function of the angle from jet axis of the top-hat jet

$$E(\theta) = \begin{cases} E_0 & \theta \leqslant \theta_c \\ 0 & \theta > \theta_c \end{cases}, \tag{1}$$

where θ_c is the half opening angle of the jet core and θ is the angle from the jet axis. The beaming-corrected kinetic energy of the jet can be calculated via $E_K = E_0(1 - \cos\theta_c) \sim E_0\frac{\theta_c^2}{2}$.

In `afterglowpy`, the energy distribution of the Gaussian jet model is defined as the following function

$$E(\theta) = \begin{cases} E_0 e^{-\frac{\theta^2}{2\theta_c}} & \theta \leqslant \theta_w \\ 0 & \theta > \theta_w \end{cases}, \tag{2}$$

where θ_w is the truncation angle of the Gaussian jets.

The power-law jet model introduces one more parameter b to describe the energy distribution as

$$E(\theta) = \begin{cases} E_0\left(1 + \frac{\theta^2}{b\theta_c^2}\right)^{-\frac{b}{2}} & \theta \leqslant \theta_w \\ 0 & \theta > \theta_w \end{cases}. \tag{3}$$

The beaming-corrected kinetic energy E_K for the Gaussian and power-law jet model can be calculated by integrating Equations (2) and (3), respectively.

`Afterglowpy` utilizes semi-analytic methods to calculate the afterglow emission and uses the trans-relativistic equation to connect the ultra-relativistic and non-relativistic phases. In addition, `afterglowpy` can capture the features of afterglow emission for different viewing angles, and also provides approximated descriptions for the jet LE. Therefore, `afterglowpy` offers a greater degree of flexibility to study the GRB afterglow emission. A detailed introduction is available in the article Ryan et al. (2020) and at the website https://github.com/geoffryan/afterglowpy.

The process of our fitting is as follows: with the observed broadband fluxes, frequencies and observation times as input, and by employing `emcee` with `afterglowpy`, we can derive a posterior distribution of parameters on properties of the jets, such as E_0, θ_v, θ_c, θ_w, b, the fraction of shock energy converted to electrons and to the magnetic field ϵ_e, ϵ_B, the spectral index of the electron distribution p, the circumburst density n_0 and the participation fraction ξ_N.

3. GRB 050820A

3.1. Data

The Swift Burst Alert Telescope (BAT) was triggered by GRB 050820A at 06:34:53 on 2005 August 20 (UT) (Page et al. 2005b). The Konus-Wind instrument also was triggered by the burst 257.948 seconds later (Pal'Shin & Frederiks 2005). The total fluence in the energy range of 20–1000 keV was $5.27^{+1.58}_{-0.69} \times 10^{-5}$ erg cm^{-2}. At redshift $z = 2.615$ (Prochaska et al. 2005; Ledoux et al. 2005), the total isotropic γ-ray energy in the energy range of 1–10^4 keV was $\sim 9.7 \times 10^{53}$ erg (Cenko et al. 2006, 2010).

The Swift X-Ray Telescope (XRT) started to observe GRB 050820A from 80 s after the BAT trigger (Page et al. 2005a). The flux density at 1 keV is calculated by adopting an average spectral index $\Gamma_X = 1.88^{+0.04}_{-0.04}$ and the fluence in the energy range of 0.3–10 keV provided by the Swift/XRT burst Analyser.[3]

We adopted optical observations presented in Cenko et al. (2006), and a correction for Galactic extinction $E(B-V) = 0.044$ mag from Schlegel et al. (1998) was made. We do not use the U-band or B-band data in the light curve modeling, since they are affected by Ly-α absorption (Madau 1995).

[3] https://www.swift.ac.uk/burst_analyser/00151207/

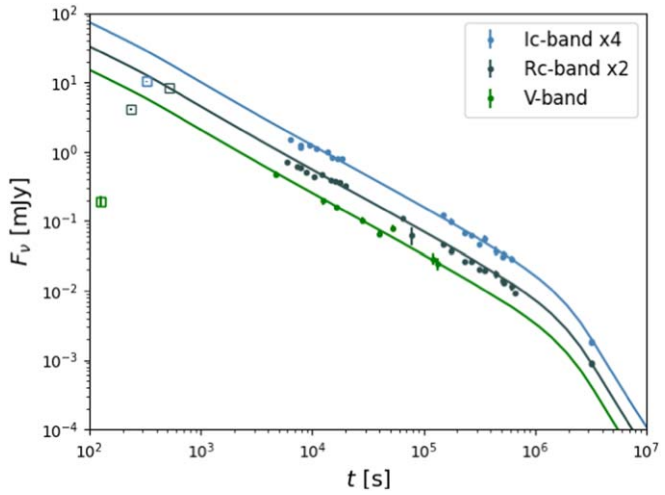

Figure 1. Observed optical data (points) of *Ic*-, *Rc*- and *V*-band and corresponding fits (lines) ignoring observations before 600 s, which are indicated by hollow squares.

Since the synchrotron self-absorption (SSA) effect is not included in `afterglowpy`, and the radio data might be affected by the SSA effect, we do not use the radio data in the modeling.

3.2. Analysis

We adopt `afterglowpy` to fit the X-ray and optical light curves using the top-hat, Gaussian and power-law jet models. In the first attempt, we ignored the optical data before $T_0 + 600$ s, since the emission is composed of both prompt emission and forward shock afterglow emission (Vestrand et al. 2006), where T_0 is the burst time. However, the predicted light curves overshoot the observed data in *V*-, *Rc*- and *Ic*-bands before $T_0 + 600$ s, as depicted in Figure 1. The reason might be that `afterglowpy` does not include an initial coasting phase (Ryan et al. 2020), which may affect the predicted light curves at very early time. Therefore, in the end, we adopt the data from $T_0 + 0.05$ days to avoid this problem. The results for different jet models and considering LE/no LE are listed in Table 1. From the table, we learn that, for top-hat jet models, the resulting parameters are similar no matter whether LE is considered or not.

GRB 050820A is a long GRB originating from the death of a massive star, for which the local circumburst density is expected to be $\sim 10^{-3}$–$10^{2}\,\mathrm{cm}^{-3}$. However, the fitted value of the circumburst medium density ($n_0 \sim 10^{-7}\,\mathrm{cm}^{-3}$) is extremely low. We note that GRB 050820A is not the only GRB for which the medium density is particularly small. The circumburst medium densities of a few GRBs, such as GRB 160509A ($2.9 \times 10^{-4}\,\mathrm{cm}^{-3}$), GRB 160625B ($9.6 \times 10^{-7}\,\mathrm{cm}^{-3}$), GRB 210619B ($6 \times 10^{-5}\,\mathrm{cm}^{-3}$) and GRB 171710A ($8.9 \times 10^{-5}\,\mathrm{cm}^{-3}$), are also constrained to be extremely low (Kangas & Fruchter 2021; Cunningham et al. 2020; Oganesyan et al. 2021). These peculiar long GRBs might originate from metal-poor stars with low mass-loss rates (Cunningham et al. 2020).

Adopting parameters for the top-hat (LE) model listed in Table 1, we calculate the light curves for the radio bands, and find out that the SSA effect is needed to avoid overshooting the radio flux. If we assume the SSA frequency to be $\nu_a = 13$ GHz, the calculated light curves can fit the observations well at the frequency of 8.46 GHz from 20 days after the burst, and do not overshoot observations at frequencies of 4.86 and 22.5 GHz. The calculated light curves for the X-ray, optical and radio bands, for the top-hat (LE) model, assuming $\xi_N = 1$ and $\nu_a = 13$ GHz, are plotted in Figure 2.[4]

The calculated spectra at three epochs of 0.2 days, 2.0 days and 7.0 days are plotted in Figure 3. From Figure 3, we ascertain that $\nu_m < \nu_o < \nu_x < \nu_c$ at 0.2 days after the burst, where ν_o and ν_x correspond to the frequencies of the optical data and the X-ray data, respectively, and ν_c and ν_m are the cooling frequency and the minimum frequency of electrons, respectively. We simply use a single power-law function of $F_\nu \propto \nu^{-\beta}$ to fit the observed spectra in Figure 3, and then check whether the value of p is consistent with that derived from `afterglowpy`. The fitted slope of the single power-law spectrum is $\beta = -0.727^{+0.023}_{-0.028}$, then the corresponding value of p is $p = -(2\beta + 1) = 2.454^{+0.054}_{-0.046}$, which is consistent with the results shown in Table 1 within the margin of error.

4. GRB 070125

4.1. Data

GRB 070125 was triggered at 07:20:42 on 2007 January 25 (UT) by space telescopes in the Inter Planetary Network (IPN) (Hurley et al. 2007). The total fluence in the energy band of 20 keV–10 MeV is $1.74 \times 10^{-4}\,\mathrm{erg\,cm}^{-2}$ detected by the Konus-Wind (Golenetskii et al. 2007; Bellm et al. 2008). Adopting the redshift $z = 1.547$ (Cenko et al. 2008), we get the isotropic γ-ray energy as 1.1×10^{54} erg (Chandra et al. 2008).

The Swift XRT started to observe this GRB at 46.7 ks after the trigger (Racusin et al. 2007). The flux density at 1 keV is calculated by adopting an average spectral index $\Gamma_X = 1.96^{+0.20}_{-0.19}$ and the fluence in the energy range of 0.3–10 keV provided by the Swift/XRT burst Analyser.[5]

We adopt the data from the ultraviolet to infrared bands corrected for Galactic extinction from Updike et al. (2008) and Chandra et al. (2008). We do not use the data of uvw2 and uvm2 bands in the `afterglowpy` fitting, since they suffer severe Ly-α absorption.

[4] The observed radio light curves in Figure 2 are not reproduced well. This might be because the early radio observations (before 20 days) are disturbed by the interstellar scintillation (Rickett et al. 1984; Rickett 1986).
[5] https://www.swift.ac.uk/burst_analyser/00020047/

Table 1
Physical Parameter Posteriors for GRB 050820A

Model	Top-hat (LE)	Gaussian (LE)	Power-law (LE)	Top-hat (free ξ_N) (LE)	Top-hat
θ_v[rad]	$0.002^{+0.001}_{-0.001}$	$0.002^{+0.001}_{-0.001}$	$0.002^{+0.001}_{-0.001}$	$0.002^{+0.001}_{-0.001}$	$0.002^{+0.001}_{-0.001}$
$\log_{10} E_0$	$55.148^{+0.081}_{-0.138}$	$55.154^{+0.082}_{-0.138}$	$55.140^{+0.072}_{-0.126}$	$55.735^{+0.640}_{-0.433}$	$55.149^{+0.081}_{-0.137}$
θ_c[rad]	$0.015^{+0.004}_{-0.002}$	$0.055^{+0.014}_{-0.018}$	$0.055^{+0.017}_{-0.018}$	$0.012^{+0.004}_{-0.003}$	$0.015^{+0.004}_{-0.002}$
θ_w[rad]		$0.015^{+0.004}_{-0.002}$	$0.015^{+0.004}_{-0.002}$		
b			$4.448^{+3.103}_{-3.040}$		
p	$2.450^{+0.009}_{-0.009}$	$2.450^{+0.009}_{-0.009}$	$2.443^{+0.009}_{-0.009}$	$2.449^{+0.009}_{-0.009}$	$2.450^{+0.009}_{-0.009}$
$\log_{10} n_0$	$-7.171^{+0.690}_{-0.076}$	$-7.173^{+0.692}_{-0.377}$	$-7.186^{+0.628}_{-0.336}$	$-7.274^{+0.862}_{-0.511}$	$-7.176^{+0.685}_{-0.373}$
$\log_{10} \epsilon_e$	$-1.659^{+0.140}_{-0.076}$	$-1.660^{+0.140}_{-0.076}$	$-1.661^{+0.127}_{-0.068}$	$-2.244^{+0.435}_{-0.643}$	$-1.660^{+0.138}_{-0.075}$
$\log_{10} \epsilon_B$	$-0.310^{+0.227}_{-0.416}$	$-0.309^{+0.227}_{-0.418}$	$-0.275^{+0.202}_{-0.378}$	$-0.443^{+0.322}_{-0.573}$	$-0.307^{+0.225}_{-0.414}$
ξ_N	1	1	1	$0.328^{+0.392}_{-0.229}$	1
η	$0.065^{+0.022}_{-0.010}$	$0.064^{+0.022}_{-0.010}$	$0.066^{+0.020}_{-0.009}$	$0.018^{+0.029}_{-0.013}$	$0.064^{+0.022}_{-0.010}$
E_{rel}[erg]	$1.691^{+0.331}_{-0.178} \times 10^{51}$	$1.681^{+0.328}_{-0.191} \times 10^{51}$	$1.632^{+0.368}_{-0.217} \times 10^{51}$	$3.981^{+5.662}_{-1.291} \times 10^{51}$	$1.695^{+0.336}_{-0.178} \times 10^{51}$
Reduced-χ^2	1.46	1.46	1.63	1.46	1.46

Note. The median posterior values with 1σ uncertainties for parameters in each case. ξ_N is set to be 1 except for the case marked with free ξ_N. LE signifies cases that consider the jet LE. No LE corresponds to cases that ignore the jet LE. The radiation efficiency is defined as $\eta = \frac{E_{\gamma,iso}}{E_{\gamma,iso}+E_{K,iso}}$, where $E_{K,iso}$ is the isotropic kinetic energy and $E_{\gamma,iso} \simeq 9.7 \times 10^{53}$ erg (Cenko et al. 2010). $E_{rel} = E_K + E_\gamma$, where E_γ is the beaming corrected γ-ray energy of the burst.

The radio data in the bands of 22.5, 14.96 and 8.46 GHz are adopted from Chandra et al. (2008). The radio data in the early time before 20 days post the burst are excluded in the fitting, since the interstellar scintillation causes short-term fluctuations of the flux in the early 20 days (Chandra et al. 2008).

The data between 1–2 days for all bands are excluded due to the existence of multi-flares (Updike et al. 2008).

4.2. Analysis

We try to fit the multi-wavelength afterglow light curves of GRB 070125 via the top-hat, Gaussian and power-law jet models using `afterglowpy`. In the beginning, we set $\xi_N = 1$; the resulting light curves do not agree with the observations well. Then we set the parameter ξ_N free, and get the resulting light curves that fit the observations better. The results are listed in Table 2, and the calculated light curves for the top-hat jet model are plotted in Figure 4. Models considering LE can explain the late optical observations better than models considering no LE. As seen from the light curves for *R*-band shown in Figure 4, the light curve for the case considering no LE (light green dashed line) overshoots the observed data or upper limits in the *R*-band after 22 days from the burst, while the light curve considering LE (light green solid line) is steeper (Rhoads 1999; Sari et al. 1999) and does not overshoot the observed data and upper limits. Compared to no LE models, LE models require a smaller isotropic kinetic energy $E_{K,iso}$, a larger radiation efficiency η, denser circumburst medium n_0 and larger ϵ_e but smaller ϵ_B. Moreover, considering LE, a larger θ_c is required.

The calculated spectra at two epochs for the top-hat (LE) model are plotted in Figure 5. As in Section 3.2, we perform the same single power-law fitting on the observed spectra, to check whether the value of p is consistent with that derived from `afterglowpy`. The fitted slope for the spectrum is $\beta = -1.056^{+0.028}_{-0.034}$ and $\beta = -1.012^{+0.017}_{-0.019}$ for 0.55 days and 2.9 days after the burst, respectively. As shown in Figure 5, the spectrum is in the regime of $\nu_m < \nu_c < \nu_o < \nu_x$ for the two epochs, then we have $p = -2\beta$, leading to the corresponding values of p as $2.112^{+0.068}_{-0.056}$ and $2.024^{+0.034}_{-0.038}$, respectively, which are very compatible with the constrained value of p in Table 2.

5. Discussion and Conclusion

5.1. The Comparison to Previous Works

GRB 050820A and GRB 070125 are very bright GRBs at high redshift. The abundant observations on these two GRBs provide us rich information to explore the nature of the afterglow. Analysis on GRB 050820A and GRB 070125 has been done in previous works. Cenko et al. (2006) used a simple analytical relationship to fit the light curves and spectra of GRB 050820A. Updike et al. (2008) and Chandra et al. (2008) analyzed multi-wavelength observations of GRB 070125. However, all of these works assumed a uniform jet, and set $\theta_v = 0$ and $\xi_N = 1$. In Chandra et al. (2008), some extreme parameters are required to explain the observations. For example, an extremely high radiation efficiency $\eta \sim 100\%$ and an extremely high electron energy fraction $\epsilon_e \sim 1$ is required in the case with a wind-like environment, and the magnetic field energy fraction $\epsilon_B \sim 1$ is required in the interstellar medium (ISM) case. Moreover, the flux in the *R*-band calculated by Chandra et al. (2008) overshoots the observations in the late time.

In this work, we fit light curves using the top-hat, Gaussian and power-law jet models to derive the posterior distributions of

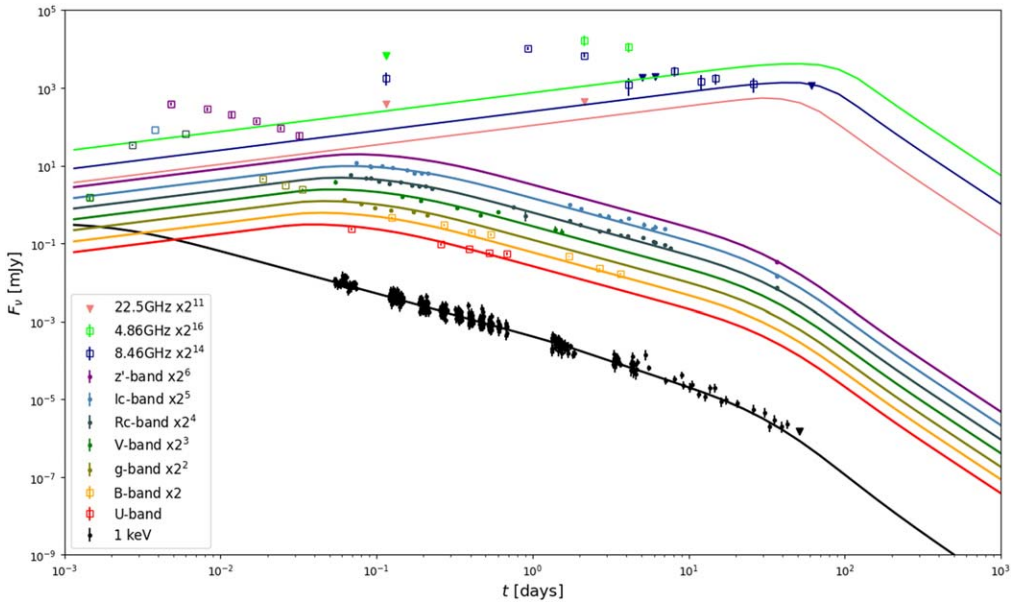

Figure 2. The observed XRT, optical and radio afterglow light curves of GRB 050820A, and the resulting light curves of the top-hat (LE) model ($\xi_N = 1$) from `afterglowpy`. The reported data of U- and B-band in Figure 2 were corrected by the factors $U = 0.4534$ and $B = 0.5440$ caused by Ly-α absorption. Downward triangles represent upper limits.

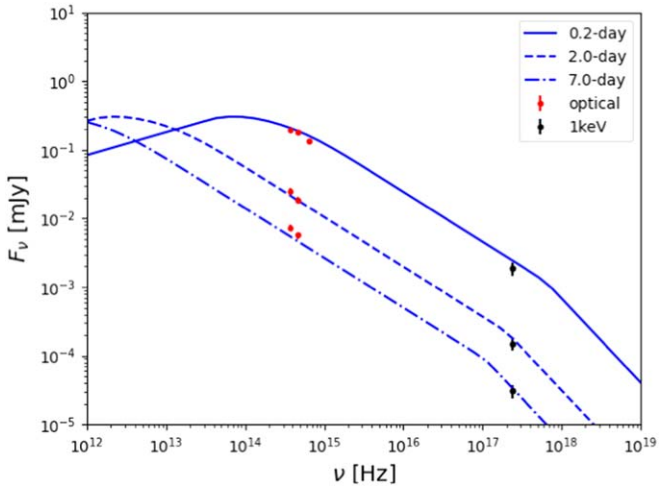

Figure 3. Observed spectral energy distribution (SED) of GRB 050820A (points) and the top-hat fits (lines) with the LE ($\xi_N = 1$) from `afterglowpy` at three epochs.

physical parameters (Figures 6 and 7). Additionally, we set θ_v and ξ_N as free parameters and take into account the impact of the LE of the jet. For GRB 070125, we find that models with free ξ_N and considering LE can fit the observations better, and no extreme parameters are needed (as shown in Table 2).

5.2. Jet Structures and Central Engines

In general, the energy budget of GRBs can be provided by the rotational energy of a magnetar or the accretion energy of a black hole. If the required jet energy of the GRB is larger than 10^{53} erg, a hyper-accreting black hole is preferred. In our work, the fitted isotropic kinetic energy of GRB 050820A is up to $\sim 10^{55}$ erg, but the jet core angle is extremely small. After being corrected by the beaming effect, the total jet energy is $\sim 10^{51}$ erg when fixing $\xi_N = 1$, and is $(2.7–9.8) \times 10^{51}$ erg if setting ξ_N free. The jet energy of GRB 070125 is $(1.5–7.3) \times 10^{51}$ erg with a high radiation efficiency, $\eta \sim 30\%–80\%$. So far, we cannot distinguish the central engine, since the required energy budget can be provided by either the rotational energy of a magnetar or the accretion energy of a black hole.

One goal of our work is to study jet structures for GRB 050820A and GRB 070125, and we find out that their jet structures are close to a top-hat jet considering the jet LE. As displayed in Table 1, the fitted values of physical parameters and the reduced-χ^2 for GRB 050820A are similar among the three jet models. For the Gaussian and power-law jet models, we have $\theta_c > \theta_w$ with the value of θ_w similar to that of the top-hat jet model, thus the Gaussian and power-law jet models are close to the top-hat jet with a similar jet opening angle as small as 0.015 rad. The density of the circumburst matter is as small as 10^{-7} cm^{-3}. The results do not change significantly if ignoring LE.

To explain the late time optical light curves of GRB 070125, the jet LE cannot be ignored. For GRB 070125, the reduced-χ^2 values are somewhat larger due to the late radio observational data. This is because when the relativistic blast wave has been decelerated to the non-relativistic phase, the LE approximation used in `afterglowpy` is not accurate enough. We have

Table 2
Physical Parameter Posteriors for GRB 070125

Model	Top-hat	Gaussian	Power-law	Top-hat (LE)	Gaussian (LE)	Power-law (LE)
$\theta_{\rm v}$[rad]	$0.033^{+0.007}_{-0.006}$	$0.031^{+0.007}_{-0.005}$	$0.001^{+0.001}_{-0.001}$	$0.051^{+0.006}_{-0.006}$	$0.051^{+0.008}_{-0.007}$	$0.054^{+0.008}_{-0.007}$
$\log_{10} E_0$	$54.226^{+0.499}_{-0.395}$	$54.422^{+0.446}_{-0.393}$	$54.174^{+0.400}_{-0.361}$	$53.488^{+0.297}_{-0.231}$	$53.656^{+0.327}_{-0.262}$	$53.536^{+0.333}_{-0.247}$
$\theta_{\rm c}$[rad]	$0.034^{+0.007}_{-0.006}$	$0.024^{+0.006}_{-0.004}$	$0.011^{+0.002}_{-0.001}$	$0.094^{+0.011}_{-0.010}$	$0.089^{+0.014}_{-0.012}$	$0.092^{+0.013}_{-0.012}$
$\theta_{\rm w}$[rad]		$0.148^{+0.092}_{-0.075}$	$0.077^{+0.013}_{-0.012}$		$0.093^{+0.015}_{-0.013}$	$0.094^{+0.014}_{-0.013}$
b			$0.594^{+0.051}_{-0.047}$			$0.023^{+0.297}_{-0.019}$
p	$2.053^{+0.011}_{-0.011}$	$2.042^{+0.011}_{-0.010}$	$2.048^{+0.011}_{-0.010}$	$2.048^{+0.014}_{-0.014}$	$2.040^{+0.012}_{-0.010}$	$2.044^{+0.013}_{-0.012}$
$\log_{10} n_0$	$-0.981^{+0.505}_{-0.414}$	$-1.009^{+0.525}_{-0.381}$	$-0.750^{+0.445}_{-0.360}$	$0.902^{+0.415}_{-0.347}$	$0.860^{+0.481}_{-0.420}$	$0.902^{+0.478}_{-0.414}$
$\log_{10} \epsilon_{\rm e}$	$-1.072^{+0.403}_{-0.496}$	$-1.128^{+0.393}_{-0.451}$	$-1.107^{+0.362}_{-0.435}$	$-0.480^{+0.218}_{-0.305}$	$-0.506^{+0.231}_{-0.339}$	$-0.482^{+0.229}_{-0.327}$
$\log_{10} \epsilon_B$	$-0.402^{+0.230}_{-0.390}$	$-0.344^{+0.206}_{-0.375}$	$-0.384^{+0.221}_{-0.391}$	$-0.690^{+0.253}_{-0.361}$	$-0.665^{+0.280}_{-0.395}$	$-0.727^{+0.296}_{-0.390}$
ξ_N	$0.154^{+0.162}_{-0.095}$	$0.105^{+0.104}_{-0.058}$	$0.098^{+0.098}_{-0.057}$	$0.121^{+0.066}_{-0.060}$	$0.117^{+0.068}_{-0.060}$	$0.124^{+0.073}_{-0.063}$
η	$0.395^{+0.223}_{-0.224}$	$0.294^{+0.213}_{-0.164}$	$0.424^{+0.204}_{-0.197}$	$0.781^{+0.077}_{-0.138}$	$0.708^{+0.108}_{-0.175}$	$0.762^{+0.088}_{-0.164}$
$E_{\rm rel}$[erg]	$1.608^{+0.904}_{-0.114} \times 10^{51}$	$2.227^{+1.299}_{-0.230} \times 10^{51}$	$2.840^{+1.101}_{-0.206} \times 10^{51}$	$6.214^{+0.839}_{-0.187} \times 10^{51}$	$5.175^{+0.872}_{-0.077} \times 10^{51}$	$6.163^{+1.130}_{-0.329} \times 10^{51}$
Reduced-χ^2				6.80	8.50	6.41

Note. The median posterior values with 1σ uncertainties for parameters in each case for GRB 070125. $E_{\gamma,\rm iso} = 1.1 \times 10^{54}$ erg (Chandra et al. 2008). Because the calculated light curves overshoot the late optical upper limits (Figure 4) for the case considering no LE, we did not calculate the corresponding reduced-χ^2.

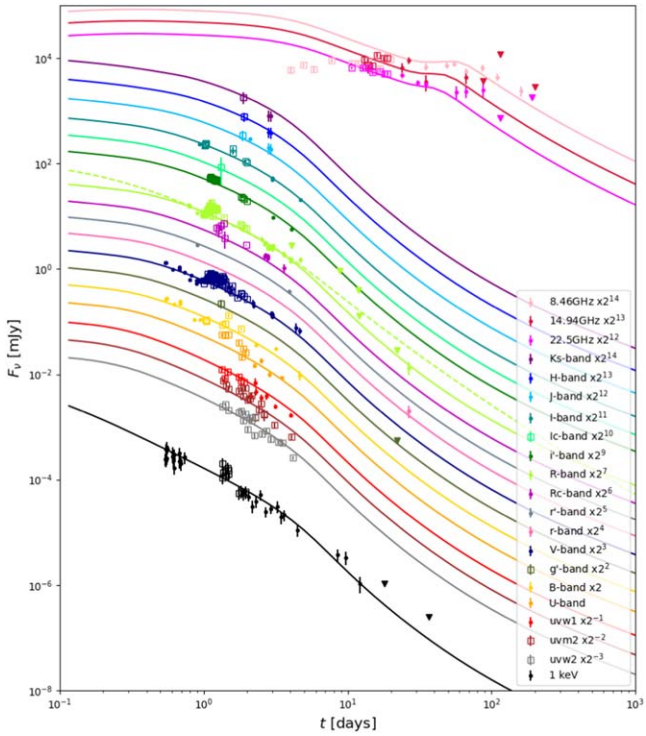

Figure 4. The observed XRT, optical and radio afterglow light curves of GRB 070125, and the resulting light curves of the top-hat (LE) model from `afterglowpy`. The light green dashed line signifies the case of no LE in the *R*-band for comparison. The optical data are adopted from Chandra et al. (2008) and Updike et al. (2008). The data of *U*, uvw1, uvw2 and uvm2 bands were corrected by these factors: $U = 0.996$, uvw1 $= 0.848$, uvw2 $= 0.7350$ and uvm2 $= 0.6834$. Downward triangles represent upper limits.

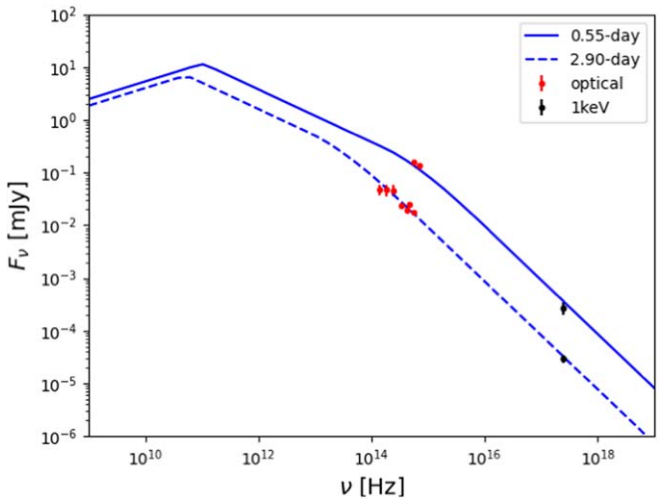

Figure 5. Observed SED of GRB 07025 and the calculated spectrum of the top-hat (LE) model from `afterglowpy` at two epochs.

$\theta_{\rm w} \simeq \theta_{\rm c}$ for the Gaussian and power-law jet models considering LE, and the value of b for the power-law jet model is extremely small, which make the jet structure also close to the top-hat jet, with a half opening angle of about 0.1 rad and the viewing angle of about 0.05 rad. The circumburst density is constrained to be about 10 $\rm cm^{-3}$, and the participation factor of electrons that are accelerated by the shock is required to be about 0.1.

Compared to the above two bursts, GRB 160625B showed some different features. Cunningham et al. (2020) found that for GRB 160625B the Gaussian jet model was more favored

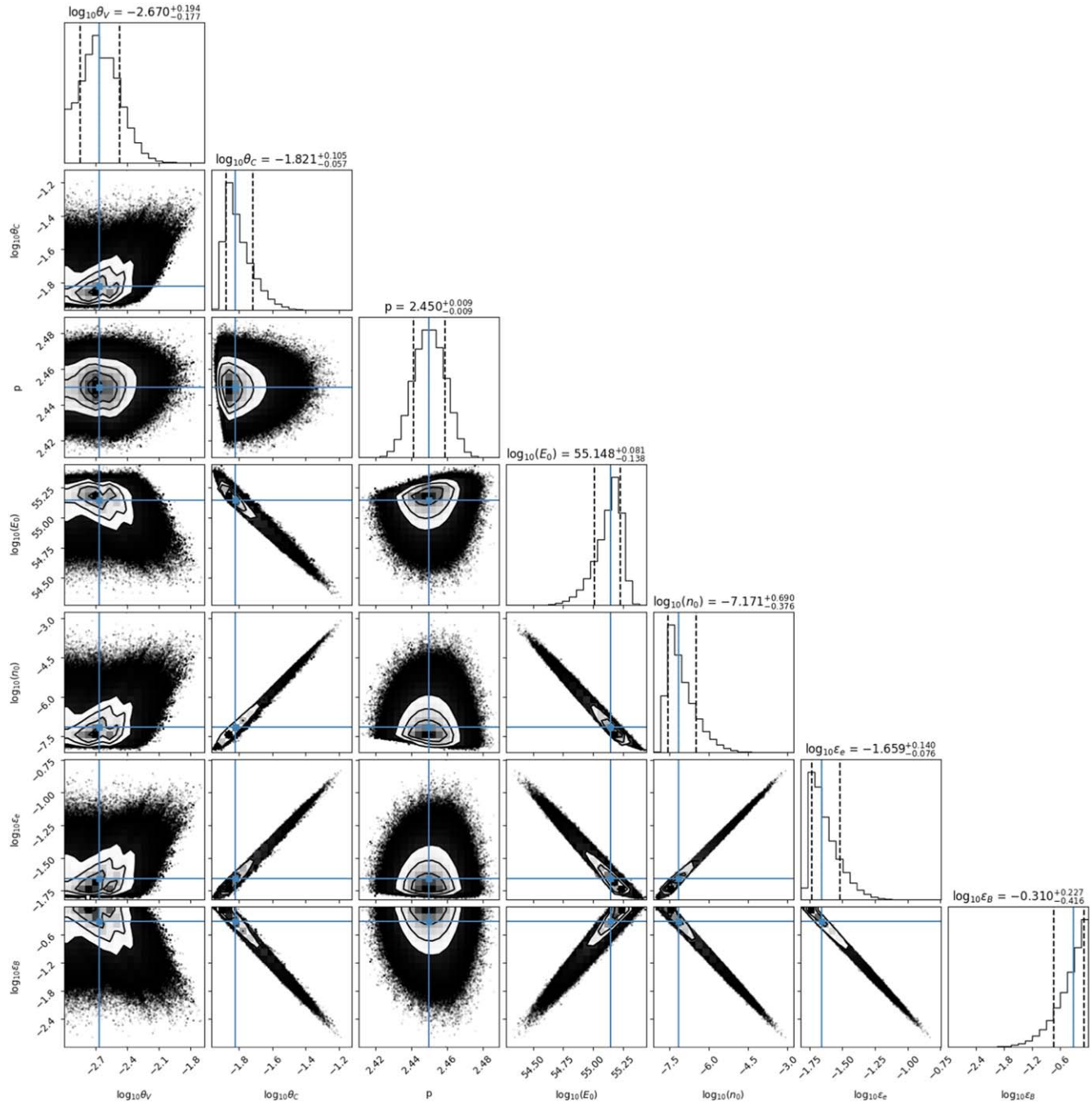

Figure 6. The posterior distribution of physical parameters of the top-hat jet (LE) model for GRB 050820A. Blue solid lines show the locations of the median values. Dashed lines signify the 16th and 84th percentiles of the distributions.

with the viewing angle $\frac{\theta_v}{\theta_c} \sim 1$ and the jet critical angle $\frac{\theta_c}{\theta_w} \sim 0.8$, while for GRB 050820A and GRB 070125, we found $\frac{\theta_v}{\theta_c} \sim 0.1$ and $\frac{\theta_v}{\theta_c} \sim 0.5$ respectively.

The jet structure may have some implications for the central engine and jet initiation/propagation. Morsony et al. (2007) performed simulations of the jet propagating through a stellar envelope and found that the top-hat jet could be generated if the progenitor star is compact and the jet injection Lorentz factor is large. Therefore, the nearly uniform jet structure of GRB 050820A and GRB 070125 suggests that these two bursts may originate from the compact stars and have large injection Lorentz factors.

We note that the viewing angles of these two GRBs are very small. This may be a selection effect since most high redshift

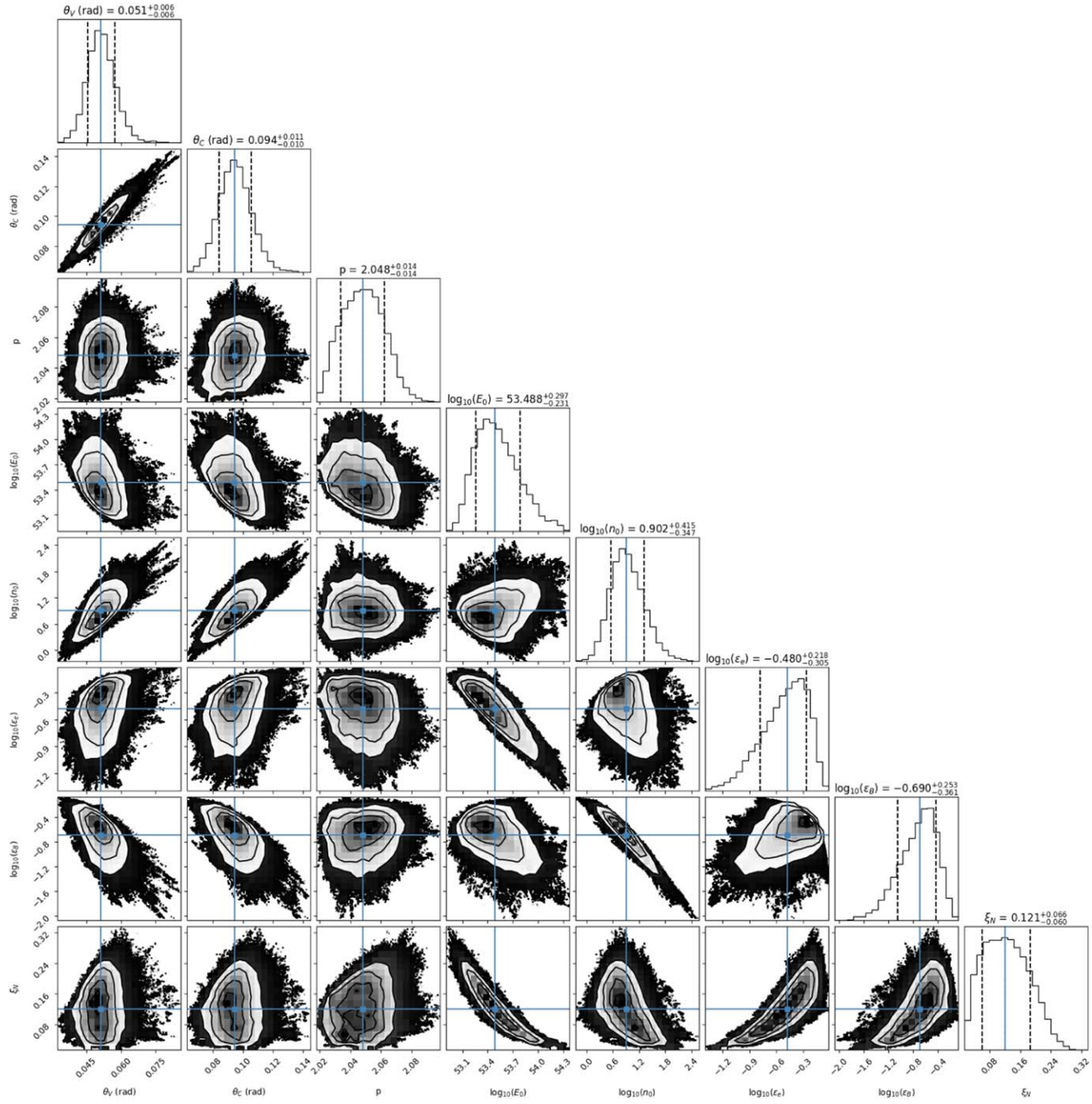

Figure 7. The posterior distribution of physical parameters of the top-hat jet (LE) model for GRB 070125.

GRBs may only be detected for small viewing angles. However, for nearby GRBs, they can be observed even for relatively large viewing angles such as GRB 170817A. Therefore, in the future, we will focus on the nearby GRBs, because in this case the viewing angle distribution and the jet structure may be even better constrained.

Acknowledgments

We gratefully thank the anonymous referee for careful reading and many important suggestions that improved this paper. This work was supported by the National Natural Science Foundation of China (NSFC, Grant Nos. 12073080, 11933010, 11921003 and 12173091) and by the Chinese

Academy of Sciences via the Key Research Program of Frontier Sciences (No. QYZDJ-SSW-SYS024).

References

Abbott, B. P., Abbott, R., Abbott, T., et al. 2017a, ApJL, 848, 1
Abbott, B. P., Abbott, R., Abbott, T., et al. 2017b, PhRvL, 119, 161101
Aghanim, N., Akrami, Y., Ashdown, M., et al. 2020, A&A, 641, A6
Alexander, K., Margutti, R., Blanchard, P., et al. 2018, ApJL, 863, L18
Bellm, E. C., Hurley, K., Pal'shin, V., et al. 2008, ApJ, 688, 491
Burns, E. 2016, GCN, 19587, 1
Cenko, S., Frail, D., Harrison, F., et al. 2010, ApJ, 711, 641
Cenko, S. B., Fox, D. B., Penprase, B. E., et al. 2008, ApJ, 677, 441
Cenko, S. B., Kasliwal, M., Harrison, F., et al. 2006, ApJ, 652, 490
Chandra, P., Cenko, S. B., Frail, D. A., et al. 2008, ApJ, 683, 924
Cunningham, V., Cenko, S. B., Ryan, G., et al. 2020, ApJ, 904, 166
Fong, W.-f., Blanchard, P., Alexander, K., et al. 2019, ApJL, 883, L1
Foreman-Mackey, D., Hogg, D. W., Lang, D., & Goodman, J. 2013, PASP, 125, 306
Ghirlanda, G., Salafia, O. S., Paragi, Z., et al. 2019, Sci, 363, 968
Golenetskii, S., Aptekar, R., Mazets, E., et al. 2007, GCN, 6049, 1
He, X.-B., Tam, P.-H. T., & Shen, R.-F. 2018, RAA, 18, 043
Hotokezaka, K., Kiuchi, K., Shibata, M., Nakar, E., & Piran, T. 2018, ApJ, 867, 95
Hurley, K., Cline, T., Mitrofanov, I., et al. 2007, GCN, 6024, 1
Kangas, T., & Fruchter, A. S. 2021, ApJ, 911, 14
Kumar, P., & Granot, J. 2003, ApJ, 591, 1075
Lamb, G., Lyman, J., Levan, A., et al. 2019, ApJL, 870, L15
Lamb, G. P., & Kobayashi, S. 2017, MNRAS, 472, 4953
Ledoux, C., Vreeswijk, P., Ellison, S., et al. 2005, GCN, 3860, 1
Madau, P. 1995, ApJ, 441, 18
Mooley, K., Deller, A., Gottlieb, O., et al. 2018, Natur, 561, 355
Morsony, B. J., Lazzati, D., & Begelman, M. C. 2007, ApJ, 665, 569
Oganesyan, G., Karpov, S., Jelínek, M., et al. 2021, arXiv:2109.00010
Page, K. L., Beardmore, A. P., Goad, M. R., et al. 2005a, GCN, 3837, 1
Page, M., Burrows, D., Beardmore, A., et al. 2005b, GCN, 3830, 1
Pal'Shin, V., & Frederiks, D. 2005, GCN, 3852, 1
Prochaska, J. X., Bloom, J. S., Wright, J. T., et al. 2005, GCN, 3833, 1
Racusin, J., Cummings, J., & Marshall, F. 2007, GCNR, 28, 1
Rhoads, J. E. 1999, ApJ, 525, 737
Rickett, B. 1986, ApJ, 307, 564
Rickett, B., Coles, W. A., & Bourgois, G. 1984, A&A, 134, 390
Ryan, G., Van Eerten, H., Piro, L., & Troja, E. 2020, ApJ, 896, 166
Sari, R., Piran, T., & Halpern, J. P. 1999, ApJL, 519, L17
Schlegel, D. J., Finkbeiner, D. P., & Davis, M. 1998, ApJ, 500, 525
Troja, E., Castro-Tirado, A. J., Becerra González, J., et al. 2019, MNRAS, 489, 2104
Updike, A. C., Haislip, J. B., Nysewander, M. C., et al. 2008, ApJ, 685 361
Uso, V. 1992, Natur, 357, 472
Vestrand, W., Wren, J., Wozniak, P., et al. 2006, Natur, 442, 172
Wei, D., & Jin, Z. 2003, A&A, 400, 415
Woosley, S. E. 1993, ApJ, 405, 273
Wu, Y., & MacFadyen, A. 2018, ApJ, 869, 55
Xu, D., Malesani, D., Fynbo, J. P. U., et al. 2016, GCN, 19600, 1